

# External Division of Two Bregman Proximity Operators for Poisson Inverse Problems

Kazuki Haishima, Kyohei Suzuki, and Konstantinos Slavakis

*Institute of Science Tokyo, Department of Information and Communications*

Emails: {haishima.k.7e90, suzuki.k.439f}@m.isct.ac.jp, slavakis@ict.eng.isct.ac.jp

**Abstract**—This paper presents a novel method for recovering sparse vectors from linear models corrupted by Poisson noise. The contribution is twofold. First, an operator defined via the external division of two Bregman proximity operators is introduced to promote sparse solutions while mitigating the estimation bias induced by classical  $\ell_1$ -norm regularization. This operator is then embedded into the already established NoLips algorithm, replacing the standard Bregman proximity operator in a plug-and-play manner. Second, the geometric structure of the proposed external-division operator is elucidated through two complementary reformulations, which provide clear interpretations in terms of the primal and dual spaces of the Poisson inverse problem. Numerical tests show that the proposed method exhibits more stable convergence behavior than conventional Kullback-Leibler (KL)-based approaches and achieves significantly superior performance on synthetic data and an image restoration problem.

**Index Terms**—Inverse problems, Poisson noise, sparse modeling, Bregman divergence, proximity operator.

## I. INTRODUCTION

Inverse problems involving discrete event counts, such as positron emission tomography (PET) imaging and photon counting, are typically corrupted by Poisson noise rather than Gaussian [1]–[3]. With  $n, m$  being positive integers, the standard task in such scenarios is to reconstruct a sparse vector  $\mathbf{x}_\diamond \in \mathbb{R}^n$  from the corrupted signal  $\mathbf{b} \in \mathbb{R}^m$  that follows the Poisson distribution with mean vector  $\mathbf{A}\mathbf{x}_\diamond$ , *i.e.*,  $\mathbf{b} \sim \text{Poisson}(\mathbf{A}\mathbf{x}_\diamond)$ , where  $\mathbf{A} \in \mathbb{R}^{m \times n}$  is a known sensing matrix, and  $\text{Poisson}(\cdot)$  acts independently on each entry of the vector  $\mathbf{A}\mathbf{x}_\diamond$ . To estimate  $\mathbf{x}_\diamond$ , a standard approach is to cast the problem as the minimization of an objective function that combines a data-fidelity term based on the celebrated Kullback-Leibler (KL) divergence with a sparsity-inducing regularizer [4], [5].

The KL divergence is a specific instance of the Bregman  $D_\phi(\cdot, \cdot)$  one, where  $\phi$  is the Boltzmann-Shannon entropy (see Section II for definitions). Owing to its asymmetry, two natural candidates arise for the data-fidelity loss: (i)  $f(\mathbf{x}) = D_\phi(\mathbf{b}, \mathbf{A}\mathbf{x})$ , which corresponds to the statistically natural formulation, and (ii)  $f(\mathbf{x}) = D_\phi(\mathbf{A}\mathbf{x}, \mathbf{b})$ , which is adopted in [6] for solving inconsistent linear systems with nonnegative data. While the latter lacks a direct Poisson-likelihood interpretation, it nonetheless provides a meaningful measure of residuals between nonnegative signals [7]. A major challenge in Poisson inverse problems is that, in both cases, the gradient of  $f(\cdot)$  fails to be Lipschitz continuous, thereby preventing standard proximal-gradient methods from offering convergence guarantees [8]. To overcome this limitation, the

NoLips algorithm [6], [9] establishes convergence guarantees by relying on a *Lipschitz-like convexity condition* in place of the standard descent lemma (see Section II for details). Algorithms based on the aforementioned data-fidelity formulations combined with  $\ell_1$ -norm regularization can be found in [6].

Notwithstanding, although these algorithms ensure convergence for Poisson inverse problems, the use of the  $\ell_1$ -norm—a convex penalty—may induce severe estimation bias by underestimating large coefficients. To mitigate this well-known issue, various nonconvex penalties have been proposed in the field of sparse optimization, including the minimax-concave (MC) penalty [10], the smoothly clipped absolute deviation (SCAD) [11], and the  $\ell_q$ -(quasi-)norm for  $q \in (0, 1)$  [12].

A popular approach for incorporating prior information, such as sparsity, into iterative algorithms is regularization via operators, commonly referred to as plug-and-play (PnP) [13], in which the proximity operator in a forward-backward-type algorithm is replaced by a “plug-in operator.” In the context of Poisson inverse problems, [14] employed the PnP strategy within the NoLips framework, where the plug-in operator is a pre-trained “black-box” neural-network denoiser. While such data-driven approaches have demonstrated promising performance, the design of mathematically explainable operators for bias reduction in Poisson inverse problems remains a fundamental challenge.

The external-division operator [15], [16], defined as an affine combination of two proximity operators with both positive and negative weights, has recently been introduced as a generalization of the firm-shrinkage operator, which corresponds to the proximity operator of the MC penalty. The external-division operator provides a flexible framework for bias reduction under the PnP strategy with convergence guarantees [13]. For instance, the effectiveness of the external division of two proximity operators associated with the octagonal shrinkage and clustering algorithm for regression (OSCAR) has been demonstrated in [15], highlighting the broad applicability of the external-division-operator framework.

This paper introduces a novel method for recovering sparse vectors from linear models corrupted by Poisson noise. The method integrates an external-division operator into the NoLips framework through the PnP strategy. The proposed external-division operator is newly constructed from two *Bregman* proximity operators, making it well suited to jointly promote sparsity and reduce estimation bias in Poisson inverse problems. To elucidate its structure, two complementary reformulations are derived. The first shows that bias reduction is realized in the primal space of the inverse problem, whereas sparsity promotion occurs in the dual space. The second reformulation further clarifies the bias-reduction mechanism by

This work was supported by the Grants-in-Aid for Scientific Research (KAKENHI) under Grant Number 25K24422.

revealing that the operator implicitly incorporates a correction term in the dual space. Finally, numerical tests corroborate the theoretical and algorithmic developments, demonstrating that the proposed framework significantly outperforms state-of-the-art KL-based methods on synthetic data and an image restoration problem.

## II. PRELIMINARIES

### A. Notation and definitions

Throughout the paper, let  $\mathbb{R}$ ,  $\mathbb{R}_+$ ,  $\mathbb{R}_{++}$ , and  $\mathbb{N}$  denote the sets of real, nonnegative real, strictly positive real, and nonnegative integer numbers, respectively. Let  $\mathbf{1}_n$  denote the all-ones vector of dimension  $n$ . For any  $\mathbf{x} \in \mathbb{R}^n$ , the  $i$ th entry of  $\mathbf{x}$  is defined by  $x_i$  or  $[\mathbf{x}]_i$ . The closure and interior of a subset  $C \subset \mathbb{R}^n$  are denoted by  $\overline{C}$  and  $\text{int } C$ , respectively.

A function  $f: \mathbb{R}^n \rightarrow (-\infty, +\infty] := \mathbb{R} \cup \{+\infty\}$  is convex if  $f(\alpha\mathbf{x} + (1 - \alpha)\mathbf{\xi}) \leq \alpha f(\mathbf{x}) + (1 - \alpha)f(\mathbf{\xi})$ , for any  $(\mathbf{x}, \mathbf{\xi}, \alpha) \in \mathbb{R}^n \times \mathbb{R}^n \times [0, 1]$ . Function  $f: \mathbb{R}^n \rightarrow (-\infty, +\infty]$  is called proper if  $\text{dom } f := \{\mathbf{x} \in \mathbb{R}^n \mid f(\mathbf{x}) < +\infty\} \neq \emptyset$ . A function  $f: \mathbb{R}^n \rightarrow (-\infty, +\infty]$  is lower-semicontinuous on  $\mathbb{R}^n$  if the level set  $\text{lev}_{\leq a} f := \{\mathbf{x} \in \mathbb{R}^n \mid f(\mathbf{x}) \leq a\}$  is closed for any  $a \in \mathbb{R}$ . Let  $\Gamma_0(\mathbb{R}^n)$  denote the set of proper lower-semicontinuous convex functions from  $\mathbb{R}^n$  to  $(-\infty, +\infty]$ . Given a proper function  $f: \mathbb{R}^n \rightarrow (-\infty, +\infty]$ , the conjugate function or Fenchel conjugate of  $f$  is defined by  $f^*: \mathbb{R}^n \rightarrow \mathbb{R} \cup \{+\infty, -\infty\}: \mathbf{u} \mapsto \sup_{\mathbf{x} \in \mathbb{R}^n} (\langle \mathbf{x}, \mathbf{u} \rangle_2 - f(\mathbf{x}))$ .

A function  $\theta \in \Gamma_0(\mathbb{R}^n)$  is essentially smooth if  $\theta$  is differentiable on  $\text{int } \text{dom } \theta$  and  $\lim_{k \rightarrow +\infty} \|\nabla \theta(\mathbf{x}_k)\|_2 = +\infty$  for every sequence  $\{\mathbf{x}_k\}_{k \in \mathbb{N}} \subset \text{int } \text{dom } \theta$  converging to a boundary point of  $\text{dom } \theta$ . A function  $\theta \in \Gamma_0(\mathbb{R}^n)$  is a Legendre function if  $\theta$  is essentially smooth and strictly convex on  $\text{int } \text{dom } \theta$  [6]. If  $\theta$  is a Legendre function,  $\nabla \theta$ , often referred to as the *mirror map*, is a bijection from the primal space  $\text{int } \text{dom } \theta$  to the dual space  $\text{int } \text{dom } \theta^*$ . The Bregman divergence with respect to a given Legendre function  $\theta: \mathbb{R}^n \rightarrow (-\infty, +\infty]$  is defined as  $D_\theta: \text{dom } \theta \times \text{int } \text{dom } \theta \rightarrow \mathbb{R}: (\mathbf{\xi}, \mathbf{x}) \mapsto \theta(\mathbf{\xi}) - \theta(\mathbf{x}) - \langle \nabla \theta(\mathbf{x}), \mathbf{\xi} - \mathbf{x} \rangle_2$ .

### B. The NoLips algorithm

Let  $f, g \in \Gamma_0(\mathbb{R}^n)$  such that (s.t.)  $f$  is continuously differentiable, but not necessarily Lipschitz continuous on  $\text{int } \text{dom } f \neq \emptyset$ . Consider the following minimization problem:

$$\min_{\mathbf{x} \in C} f(\mathbf{x}) + g(\mathbf{x}), \quad (1)$$

where  $C$  is a closed convex set with nonempty interior. To address the lack of Lipschitz continuity of  $\nabla f$ , the NoLips algorithm was introduced in [6]. NoLips replaces the Euclidean distance of the proximal gradient algorithm with the Bregman divergence  $D_h$  for a Legendre function  $h$  chosen so that  $C = \overline{\text{dom } h}$ . Specifically, the general update rule of the NoLips algorithm is given by:

$$\mathbf{x}_{k+1} = \text{Prox}_{\lambda g}^h(\nabla h^*(\nabla h(\mathbf{x}_k) - \lambda \nabla f(\mathbf{x}_k))), \quad (2)$$

where  $\lambda \in \mathbb{R}_{++}$  is the step size. Here, the *Bregman proximity operator* of  $g$  of index  $\gamma \in \mathbb{R}_{++}$  is defined as

$$\begin{aligned} \text{Prox}_{\gamma g}^h: \text{int } \text{dom } h &\rightarrow \mathbb{R}^n \\ &: \mathbf{z} \mapsto \underset{\mathbf{\xi} \in \mathbb{R}^n}{\text{argmin}} (g(\mathbf{\xi}) + \gamma^{-1} D_h(\mathbf{\xi}, \mathbf{z})). \end{aligned} \quad (3)$$

Specifically, when  $h: \mathbf{x} \mapsto (1/2)\|\mathbf{x}\|_2^2$ , the Bregman divergence reduces to the squared Euclidean distance, and the Bregman proximity operator becomes the standard proximity operator [17]

$$\text{Prox}_{\gamma g}: \mathbb{R}^n \rightarrow \mathbb{R}^n: \mathbf{z} \mapsto \underset{\mathbf{\xi} \in \mathbb{R}^n}{\text{argmin}} \left( g(\mathbf{\xi}) + \frac{1}{2\gamma} \|\mathbf{z} - \mathbf{\xi}\|_2^2 \right). \quad (4)$$

The convergence of the NoLips algorithm is analyzed under a *Lipschitz-like convexity condition*, stated as:

$$\exists L \in \mathbb{R}_{++} \text{ s.t. } Lh - f \text{ is convex on } \text{int } \text{dom } h. \quad (5)$$

Let now the Boltzmann-Shannon entropy  $\phi: \mathbb{R}_+^m \rightarrow \mathbb{R}: \mathbf{u} \mapsto \sum_{j=1}^m u_j \log u_j$ —known to be of Legendre type—where  $0 \log 0 := 0$ . Under the light of (1), the following two formulations were introduced in [6] to address Poisson inverse problems. Note here that  $h$  is a Legendre function chosen to ensure  $C = \overline{\text{dom } h}$  and to satisfy (5), and it can be distinct from  $\phi$  used in the data-fidelity term  $f$ .

- (i)  $f(\mathbf{x}) := D_\phi(\mathbf{b}, \mathbf{Ax})$  and  $g(\mathbf{x}) := \|\mathbf{x}\|_1$ . The composite loss of (1) corresponds to Poisson likelihood maximization. In this case, (5) is satisfied by choosing Burg's entropy as  $h$ , i.e.,  $h: \mathbb{R}_{++}^n \rightarrow \mathbb{R}: \mathbf{x} \mapsto -\sum_{j=1}^n \log x_j$  [6, Lemma 7].
- (ii)  $f(\mathbf{x}) := D_\phi(\mathbf{Ax}, \mathbf{b})$  and  $g(\mathbf{x}) := \|\mathbf{x}\|_1$ . This formulation is in general appropriate for solving inconsistent nonnegative linear-system inverse problems [7]. In this case, (5) is satisfied by choosing the Boltzmann-Shannon entropy as  $h$ , i.e.,  $h: \mathbb{R}_+^n \rightarrow \mathbb{R}: \mathbf{x} \mapsto \sum_{j=1}^n x_j \log x_j$  [6, Lemma 8].

### C. The external-division operator

The external-division operator [15], [16] is defined as the following affine combination of two proximity operators (4):

$$\Delta_\omega := \omega \text{Prox}_{g_1} - (\omega - 1) \text{Prox}_{g_2}, \quad (6)$$

where  $\omega > 1$  and  $g_1, g_2 \in \Gamma_0(\mathbb{R}^n)$ . A specific example is the firm-shrinkage operator defined  $\forall \gamma, \tau$ , with  $\gamma > \tau > 0$ , as

$$\text{firm}_{\tau, \gamma}: \mathbb{R} \rightarrow \mathbb{R}: x \mapsto \begin{cases} x, & |x| \geq \gamma, \\ \text{sgn}(x) \frac{\gamma(|x| - \tau)}{\gamma - \tau}, & |x| \in [\tau, \gamma], \\ 0, & |x| < \tau, \end{cases}$$

where  $\text{sgn}(\cdot)$  denotes the standard sign function. Indeed, the firm-shrinkage operator can be expressed as the external division of two soft-shrinkage operators (i.e., two proximity operators (4) of the  $\ell_1$ -norm) [15, Proposition 1]:

$$\text{firm}_{\tau, \gamma} = \frac{\gamma}{\gamma - \tau} \text{soft}_\tau - \frac{\tau}{\gamma - \tau} \text{soft}_\gamma, \quad (7)$$

where,  $\text{soft}_\gamma: \mathbb{R} \rightarrow \mathbb{R}: x \mapsto \text{sgn}(x) \max\{|x| - \gamma, 0\}$ ,  $\forall \gamma \in \mathbb{R}_{++}$ . The firm-shrinkage operator corresponds to the identity mapping for inputs of sufficiently large size, and hence induces nearly unbiased estimates [10].

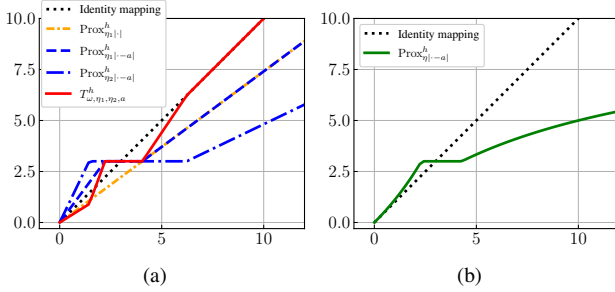


Fig. 1. (a) The difference between the proposed  $T_{\omega,\eta_1,\eta_2,a}^h$  and the standard Bregman proximity operator  $\text{Prox}_{\|\cdot-a\|_1}^h$ , where  $h(\cdot)$  is the Boltzmann-Shannon entropy, and  $\eta_1 = 0.3$ ,  $\omega = 2$ ,  $a = 3$ . Unlike the proposed  $T_{\omega,\eta_1,\eta_2,a}^h$ , the standard Bregman proximity operator leads to estimation bias for sufficiently large inputs. (b) The standard Bregman proximity operator  $\text{Prox}_{\eta\| \cdot -a\|_1}^h$  with Burg's entropy  $h(\cdot)$  for  $a = 3$  and  $\eta = 0.1$ .

### III. MAIN RESULTS

First, the definition in Section II-C is extended to encompass the external division of Bregman proximity operators. The resulting operator is then incorporated into the NoLips algorithm via a plug-and-play (PnP) strategy to address Poisson inverse problems. Two complementary reformulations of the proposed operator are presented, providing clear structural interpretations. All theoretical results are stated without proof due to space limitations; complete proofs are deferred to a future publication.

#### A. External division of two Bregman proximity operators

To reduce the estimation bias caused by the  $\ell_1$ -norm, this paper extends the discussion in Section II-C by defining the external division of two Bregman proximity operators as follows: for  $\omega, \eta_1, \eta_2, a \in \mathbb{R}_{++}$ , with  $\omega > 1$  and  $\eta_2 > \eta_1$ , and with  $h(\cdot)$  being the Boltzmann-Shannon entropy, let

$$T_{\omega,\eta_1,\eta_2,a}^h := \omega \text{Prox}_{\eta_1\| \cdot -a\mathbf{1}_n \|_1}^h - (\omega - 1) \text{Prox}_{\eta_2\| \cdot -a\mathbf{1}_n \|_1}^h. \quad (8)$$

Here, the shifted  $\ell_1$ -norm by  $a\mathbf{1}_n$  is employed to induce sparsity around  $a$ . It is empirically shown in Section IV that setting sufficiently small  $a > 0$  yields better reconstruction performance than  $a = 0$ . The following proposition provides the explicit form of  $T_{\omega,\eta_1,\eta_2,a}^h$ .

*Proposition 1:* Let  $\eta_2 := \log((\omega - 1)/(\omega e^{-\eta_1} - 1))$ . Then, for any  $\mathbf{x} \in \text{int dom } h$ , the  $i$ th entry of  $T_{\omega,\eta_1,\eta_2,a}^h(\mathbf{x})$  in (8),  $\forall i \in \{1, 2, \dots, n\}$ , takes the following explicit form:

$$[T_{\omega,\eta_1,\eta_2,a}^h(\mathbf{x})]_i = \begin{cases} (\omega e^{\eta_1} - (\omega - 1)\kappa) x_i, & x_i \in [0, a\kappa^{-1}], \\ \omega e^{\eta_1} x_i - (\omega - 1)a, & x_i \in [a\kappa^{-1}, a e^{-\eta_1}], \\ a, & x_i \in [a e^{-\eta_1}, a e^{\eta_1}], \\ \omega e^{-\eta_1} x_i - (\omega - 1)a, & x_i \in (a e^{\eta_1}, a\kappa], \\ x_i, & x_i > a\kappa, \end{cases} \quad (9)$$

where  $\kappa := (\omega - 1)/(\omega e^{-\eta_1} - 1)$ .

Notice that setting  $a = 0$  in (9) yields the trivial identity mapping  $T_{\omega,\eta_1,\eta_2,a}^h(\mathbf{x}) = \mathbf{x}$ ,  $\forall \mathbf{x} \in \text{int dom } h$ , and, hence, the proposed mapping possesses no sparsity-inducing capability. Moreover, whenever  $x_i$  is sufficiently large, (9) shows that

#### Algorithm 1 NoLips with external-division operator

---

Arbitrarily fix  $\mathbf{x}_0 \in \mathbb{R}^n$ . Choose  $\lambda, \eta_1 \in \mathbb{R}_{++}$ ,  $\omega > 1$ , and  $\eta_2 := \log((\omega - 1)/(\omega e^{-\eta_1} - 1))$ . Set  $f(\cdot) := D_\phi(\mathbf{A} \cdot, \mathbf{b})$ .

- 1: **for**  $k = 0, 1, 2, \dots$  **do**
- 2:    $\mathbf{x}_{k+1} := T_{\omega,\eta_1,\eta_2,a}^h(\nabla h^*(\nabla h(\mathbf{x}_k) - \lambda \nabla f(\mathbf{x}_k)))$ .
- 3: **end for**

---

$[T_{\omega,\eta_1,\eta_2,a}^h(\mathbf{x})]_i = x_i$ . Hence, the proposed operator behaves like the identity one for all sufficiently large inputs, thereby mitigating estimation bias, in contrast to standard Bregman proximity operators. Figure 1 illustrates the marked difference between the proposed  $T_{\omega,\eta_1,\eta_2,a}^h$  and the classical Bregman proximity operators.

Algorithm 1 summarizes the proposed framework which employs the PnP strategy [13], i.e., the proposed (8) replaces the standard Bregman proximity operator in the NoLips algorithm (2).

*Remark 1:* Algorithm 1 adopts  $f(\mathbf{x}) := D_\phi(\mathbf{A}\mathbf{x}, \mathbf{b})$ , with  $\phi(\cdot)$  chosen to be the Boltzmann-Shannon entropy, rather than  $f(\mathbf{x}) := D_\phi(\mathbf{b}, \mathbf{A}\mathbf{x})$ . These choices are motivated by the following reasons.

- Because  $\mathbf{x}$  is assumed sparse,  $\mathbf{A}\mathbf{x}$  may contain zero entries. Considering that  $D_\phi$  is defined on  $\mathbb{R}_+^n \times \mathbb{R}_{++}$  for the Boltzmann-Shannon entropy  $\phi$ ,  $D_\phi(\mathbf{b}, \mathbf{A}\mathbf{x})$  is not well defined if zeroes appear in the second argument of  $D_\phi(\cdot, \cdot)$ . In contrast,  $D_\phi(\mathbf{A}\mathbf{x}, \mathbf{b})$  is well defined, even if zeroes appear in its first argument, under the convention  $0 \log 0 = 0$ .
- To construct an external-division operator that emulates the identity mapping for large-magnitude inputs, and thereby achieves bias reduction, the two constituent Bregman proximity operators in (8) should exhibit a piecewise linear structure. As shown in Figure 1a, the operator  $\text{Prox}_{\|\cdot-a\|_1}^h$  with Boltzmann-Shannon entropy  $h = \phi$  indeed exhibits a piecewise linear structure, whereas the corresponding operator with Burg's entropy  $h$ , shown in Figure 1b, does not.

#### B. Two interpretations of the external-division operator

In this section, two different reformulations of the proposed operator defined in (8) are provided. First, a decomposition of the Bregman proximity operator associated with the Boltzmann-Shannon entropy is shown in the following proposition.

*Proposition 2:* Let  $\tilde{a} := \log a + 1$  and  $h$  be the Boltzmann-Shannon entropy. Then,

$$\text{Prox}_{\eta\| \cdot -a\mathbf{1}_n \|_1}^h = \nabla h^* \circ \text{Prox}_{\eta\| \cdot -\tilde{a}\mathbf{1}_n \|_1}^h \circ \nabla h. \quad (10)$$

*Corollary 1:* Let  $\tilde{a} := \log a + 1$ . Then, the proposed external-division operator (8) takes the following equivalent form:

$$T_{\omega,\eta_1,\eta_2,a}^h = \omega \nabla h^* \circ \text{Prox}_{\eta_1\| \cdot -\tilde{a}\mathbf{1}_n \|_1}^h \circ \nabla h - (\omega - 1) \nabla h^* \circ \text{Prox}_{\eta_2\| \cdot -\tilde{a}\mathbf{1}_n \|_1}^h \circ \nabla h. \quad (11)$$

Noting that  $\nabla h^* = (\nabla h)^{-1}$  and that  $\nabla h$  acts as a mirror map, Corollary 1 provides a clear geometric interpretation of the action of  $T_{\omega,\eta_1,\eta_2,a}^h(\mathbf{x})$  on an input vector  $\mathbf{x} \in \text{int dom } h$ : **(i)**  $\mathbf{x}$  is mapped to the dual space via  $\nabla h$ ; **(ii)** two shifted soft-shrinkage operators with different thresholds are applied

in the dual space; **(iii)** the resulting points are mapped back to the original primal space via  $(\nabla h)^{-1}$ ; and **(iv)** an affine combination of these two points is computed in the primal space. While sparsity is induced in the dual space through standard soft-shrinkage operators, bias reduction is achieved in the primal space via a simple affine combination.

Another interpretation of the mapping (8) is provided by the following proposition. To simplify the discussion, the Boltzmann–Shannon entropy  $h$  is assumed to act on scalars, that is,  $h: \mathbb{R}_+ \rightarrow \mathbb{R}$ . For notational consistency with the preceding discussion, and with a slight abuse of notation,  $\nabla h$  denotes the classical derivative  $h'$ .

*Proposition 3:* Let  $\tilde{a} := \log a + 1$ , and

$$S: \mathbb{R} \rightarrow \mathbb{R}$$

$$: u \mapsto S_1(u) + \log [\omega (1 - \exp (S_2(u) - S_1(u)))], \quad (12a)$$

where

$$S_1: \mathbb{R} \rightarrow \mathbb{R}: u \mapsto \text{Prox}_{\eta_1| \cdot - \tilde{a}|}(u), \quad (12b)$$

$$S_2: \mathbb{R} \rightarrow \mathbb{R}: u \mapsto \text{Prox}_{\eta_2| \cdot - \tilde{a}|}(u) + \log((\omega - 1)/\omega). \quad (12c)$$

Assume that  $x_i \geq a \exp(-\eta_1)$ . This assumption together with  $\eta_2 > \eta_1$  ensures that  $1 - \exp(S_2(\nabla h(x_i)) - S_1(\nabla h(x_i))) \in \mathbb{R}_{++}$ , so that  $S(\nabla h(x_i))$  is well-defined. Then, the following holds true:

$$[T_{\omega, \eta_1, \eta_2, a}^h(\mathbf{x})]_i = (\nabla h^* \circ S \circ \nabla h)(x_i). \quad (12d)$$

Result (12d) provides insight into the bias-reduction mechanism of  $T_{\omega, \eta_1, \eta_2, a}^h$  from the perspective of the dual space. In light of (10), the standard one-dimensional Bregman proximity operator can be written as  $\text{Prox}_{\eta| \cdot - a|}^h = \nabla h^* \circ S_1 \circ \nabla h$ , implying that  $\nabla h$  is shrunk by  $S_1$  in the dual space. In contrast,  $T_{\omega, \eta_1, \eta_2, a}^h$  replaces  $S_1$  with  $S$  by incorporating the correction term  $\log[\omega(1 - \exp(S_2(u) - S_1(u)))]$ . This correction term counteracts the shrinkage induced by  $S_1$  for an appropriate choice of  $\eta_2$ . In particular, when  $\eta_2 := \log((\omega - 1)/(\omega e^{-\eta_1} - 1))$ , it can be shown that  $S(u) = u$  for sufficiently large  $u$ . This interpretation not only clarifies the bias-reduction mechanism of the proposed operator in the dual space, but also suggests a possible route toward establishing convergence guarantees for Algorithm 1 in future work.

#### IV. NUMERICAL TESTS

##### A. Synthetic data

Observed data are modeled as  $\mathbf{b} \sim \text{Poisson}(\mathbf{A}\mathbf{x} + \boldsymbol{\epsilon})$ , where  $\boldsymbol{\epsilon} \in \mathbb{R}_+^m$  represents background counts, such as dark current in a charge-coupled-device (CCD) camera [18]. Following [19], the sensing matrix  $\mathbf{A}$  gathers IID entries taking values 0 or  $1/m$  with equal probability. The non-zero entries of the sparse ground-truth vector  $\mathbf{x}_\diamond$  are drawn uniformly from  $[0, k]$  with a given  $k \in \mathbb{R}_{++}$  to evaluate performance under high-variance conditions. The parameter  $\rho$  is defined here as (number of non-zero entries of  $\mathbf{x}_\diamond$ )/ $n$ . The background vector  $\boldsymbol{\epsilon}$  is set equal to the all-ones vector  $\mathbf{1}_m$ .

The proposed method is evaluated against two conventional approaches based on the NoLips framework [6]: **(i)** a method that minimizes  $D_\phi(\mathbf{A}\mathbf{x}, \mathbf{b}) + \|\mathbf{x}\|_1$ , referred to as reverse (R-)KL, and **(ii)** a method that minimizes  $D_\phi(\mathbf{b}, \mathbf{A}\mathbf{x}) + \|\mathbf{x}\|_1$ , referred to as forward (F-)KL. To ensure numerical stability,

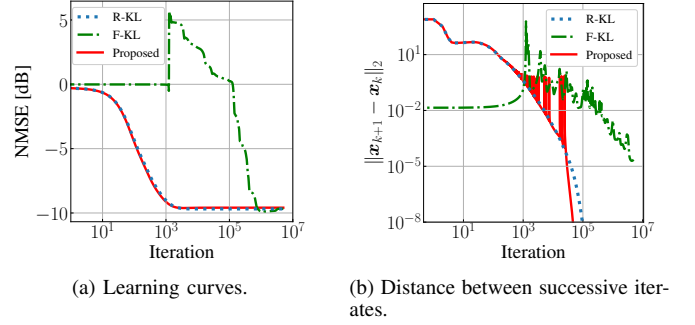


Fig. 2. Convergence behavior for  $m = 100$ ,  $n = 150$ , and  $\rho = 0.1$ .

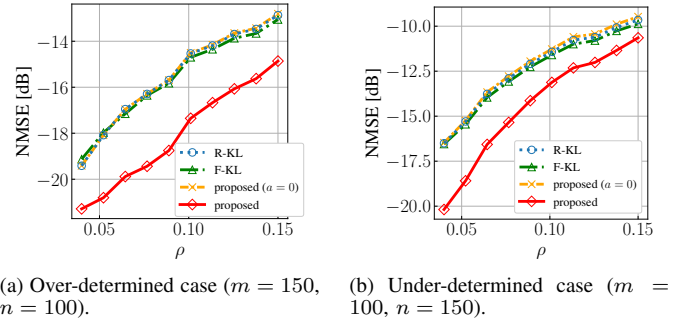


Fig. 3. NMSE as a function of  $\rho$  for (a) the over-determined case and (b) the under-determined case.

a small positive constant is added to the arguments of the logarithms. Performance is assessed using the normalized mean squared error (NMSE), defined as  $\|\hat{\mathbf{x}} - \mathbf{x}_\diamond\|_2 / \|\mathbf{x}_\diamond\|_2$ , where  $\hat{\mathbf{x}}$  denotes an estimate of  $\mathbf{x}_\diamond$ . For all methods, hyperparameters are selected via grid search to achieve the best reconstruction performance.

Figure 2a illustrates the convergence behavior for  $m = 100$ ,  $n = 150$ , and  $\rho = 0.1$ . The F-KL approach requires approximately  $1.0 \times 10^6$  iterations to converge, whereas both R-KL and the proposed method reach a steady state in fewer than  $10^4$  iterations. This disparity arises from the step-size selection in the NoLips framework: the upper bound for the F-KL step-size depends on  $1/\|\mathbf{b}\|_1$ , which becomes small as  $\|\mathbf{x}\|_2$  increases. In contrast, R-KL admits a step size that depends on  $\mathbf{A}$  and remains independent of  $\|\mathbf{x}\|_2$ , thereby enabling substantially faster convergence. Figure 2b indicates that F-KL exhibits instability, with  $\|\mathbf{x}_{k+1} - \mathbf{x}_k\|_2$  often fluctuating above  $10^{-4}$ . In contrast, the NMSE for the proposed method and R-KL reaches a steady state when  $\|\mathbf{x}_{k+1} - \mathbf{x}_k\|_2$  drops below  $10^{-4}$ .

Figure 3 reports the average NMSE over 500 trials for both over- and under-determined settings. Guided by the previous discussion, the stopping criterion is set to  $\|\mathbf{x}_{k+1} - \mathbf{x}_k\|_2 \leq 10^{-4}$  for all methods. To account for the substantial differences in convergence speed, the maximum number of iterations is set to  $10^4$  for R-KL and the proposed method, and to  $5 \times 10^6$  for F-KL, enabling a fair comparison under realistic computational budgets. The proposed method consistently achieves much lower NMSE than both F-KL and R-KL in both over- and under-determined regimes. In addition, the proposed method is compared with its non-translated counterpart ( $a = 0$ ). Since the case  $a = 0$  reduces to the identity mapping, it fails to induce sparsity effectively. The pronounced performance gap

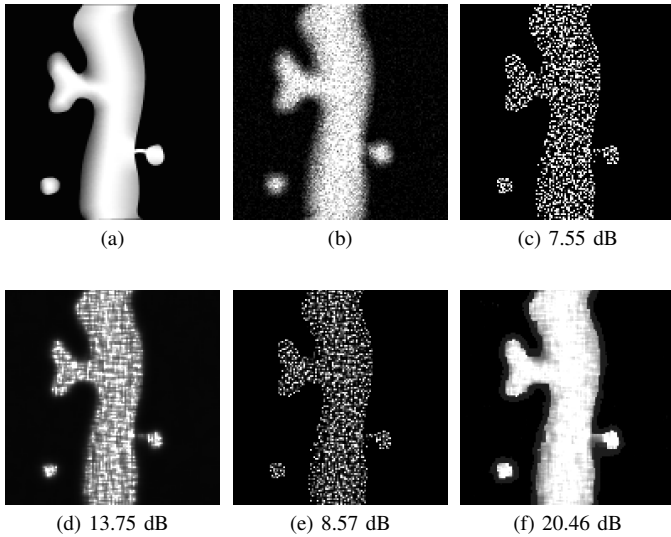


Fig. 4. (a) Original, (b) Blurred and noisy, (c) R-KL, (d) F-KL, (e) proposed method ( $a = 0$ ), and (f) proposed method ( $a > 0$ ).

confirms that the translation operation is essential for bias reduction and accurate estimation.

### B. Image restoration

A phantom image of a neuron with a mushroom-shaped spine [20] is used as the ground-truth image (Figure 4a), with  $\mathbf{x}_\diamond$  denoting its vectorized form, where  $n$  is the number of pixels. The observed image (Figure 4b) is generated by blurring the original image using a  $7 \times 7$  moving-average window and subsequently corrupting the blurred image with Poisson noise. The restored images are shown in Figures 4c–4f, with intensities normalized so that the minimum and maximum values are 0 and 30, respectively.

Performance is evaluated using the peak signal-to-noise ratio (PSNR), defined as  $\text{PSNR} := L^2 / ((1/n) \|\hat{\mathbf{x}} - \mathbf{x}_\diamond\|_2^2)$ , where  $L := 30$  denotes the maximum intensity of  $\mathbf{x}_\diamond$ . Since F-KL suffers from excessively small step sizes, its step size is carefully tuned to achieve the best possible performance. Even so, the restored image produced by F-KL exhibits visible artifacts, likely due to slow convergence. The result obtained by R-KL appears overly sparse and nonsmooth, reflecting an under-estimation of large coefficients. In contrast, the proposed method produces a relatively smooth image even without total variation (TV) regularization, effectively preserving both large and intermediate signal intensities. Finally, a comparison with the non-translated counterpart ( $a = 0$ ) highlights that careful tuning of  $a$  is crucial for the proposed operator to achieve effective bias reduction.

### V. CONCLUSIONS

In this study, a novel reconstruction method for Poisson inverse problems was proposed by integrating an external-division operator into the NoLips framework. The proposed operator was defined through the external division of two Bregman proximity operators and was designed to coincide with the identity mapping for large-magnitude inputs, thereby effectively reducing the estimation bias induced by  $\ell_1$ -norm regularization. Two reformulations of the proposed operator

were presented to provide structural interpretations. Specifically, the first reformulation revealed the separation between sparsity-inducing and bias-reducing operations, while the second reformulation elucidated the bias-reduction mechanism from the perspective of the dual space associated with the Poisson inverse problem. Numerical tests demonstrated the effectiveness of the proposed method, showing superior reconstruction accuracy compared to existing approaches on synthetic data and an image restoration problem. Future work includes a convergence analysis of the proposed method.

### REFERENCES

- [1] C. Rossignol, F. Sureau, É. Chouzenoux, C. Comtat, and J.-C. Pesquet, “A Bregman majorization–minimization framework for PET image reconstruction,” in *Proc. IEEE Int. Conf. Image Process. (ICIP)*, 2022, pp. 1736–1740.
- [2] A. Donath, A. Siemiginowska, V. L. Kashyap, D. A. van Dyk, and D. Burke, “Joint deconvolution of astronomical images in the presence of Poisson noise,” *Astron. J.*, vol. 168, no. 4, pp. 182, 2024.
- [3] M. Bertero, P. Boccacci, G. Desiderà, and G. Vicidomini, “Image deblurring with Poisson data: From cells to galaxies,” *Inverse Problems*, vol. 25, no. 12, 2009, Art. no. 123006.
- [4] Z. T. Harmany, R. F. Marcia, and R. M. Willett, “This is SPIRAL-TAP: Sparse Poisson intensity reconstruction algorithms—theory and practice,” *IEEE Trans. Image Process.*, vol. 21, no. 3, pp. 1084–1096, 2011.
- [5] M. Essafri, L. Calatroni, and E. Soubies, “On  $\ell_0$  Bregman-relaxations for Kullback-leibler sparse regression,” in *Proc. Int. Workshop Mach. Learn. Signal Process. (MLSP)*. IEEE, 2024, pp. 1–6.
- [6] H. H. Bauschke, J. Bolte, and M. Teboulle, “A descent lemma beyond Lipschitz gradient continuity: First-order methods revisited and applications,” *Math. Oper. Res.*, vol. 42, pp. 330–348, 2017.
- [7] I. Csiszar, “Why least squares and maximum entropy? An axiomatic approach to inference for linear inverse problems,” *Ann. Statist.*, vol. 19, no. 4, pp. 2032–2066, 1991.
- [8] A. Beck and M. Teboulle, “A fast iterative shrinkage-thresholding algorithm for linear inverse problems,” *SIAM J. Imaging Sci.*, vol. 2, no. 1, pp. 183–202, 2009.
- [9] J. Bolte, S. Sabach, M. Teboulle, and Y. Vaisbourd, “First order methods beyond convexity and Lipschitz gradient continuity with applications to quadratic inverse problems,” *SIAM J. Optim.*, vol. 28, no. 3, pp. 2131–2151, 2018.
- [10] C. H. Zhang, “Nearly unbiased variable selection under minimax concave penalty,” *Ann. Statist.*, vol. 38, no. 2, pp. 894–942, Apr. 2010.
- [11] J. Fan and R. Li, “Variable selection via nonconcave penalized likelihood and its oracle properties,” *J. Amer. Stat. Assoc.*, vol. 96, no. 456, pp. 1348–1360, 2001.
- [12] R. Chartrand, “Exact reconstruction of sparse signals via nonconvex minimization,” *IEEE Signal Process. Lett.*, vol. 14, no. 10, pp. 707–710, Oct. 2007.
- [13] S. V. Venkatakrishnan, C. A. Bouman, and B. Wohlberg, “Plug-and-play priors for model based reconstruction,” in *Proc. IEEE Global Conference on Signal and Information Processing (GlobalSIP)*, 2013, pp. 945–948.
- [14] S. Hurault, U. Kamilov, A. Leclaire, and N. Papadakis, “Convergent Bregman plug-and-play image restoration for Poisson inverse problems,” *Adv. Neural Inf. Process. Syst. (NeurIPS)*, vol. 36, pp. 27251–27280, 2023.
- [15] K. Suzuki and M. Yukawa, “External division of two proximity operators—Part I: Debiased feature grouping,” *IEEE Trans. Signal Process.*, vol. 74, pp. 150–166, 2026.
- [16] K. Suzuki and M. Yukawa, “External division of two proximity operators—Part II: Generalization and properties,” *IEEE Trans. Signal Process.*, vol. 74, pp. 167–182, 2026.
- [17] H. H. Bauschke and P. L. Combettes, *Convex Analysis and Monotone Operator Theory in Hilbert Spaces*, Springer, New York, 2nd edition, 2017.
- [18] D. L. Snyder, A. M. Hammoud, and R. L. White, “Image recovery from data acquired with a charge-coupled-device camera,” *J. Opt. Soc. Am. A*, vol. 10, no. 5, pp. 1014–1023, 1993.
- [19] M. Raginsky, R. M. Willett, Z. T. Harmany, and R. F. Marcia, “Compressed sensing performance bounds under Poisson noise,” *IEEE Trans. Signal Process.*, vol. 58, no. 8, pp. 3990–4002, 2010.
- [20] F.-X. Dupé, J. M. Fadili, and J.-L. Starck, “A proximal iteration for deconvolving Poisson noisy images using sparse representations,” *IEEE Trans. Image Process.*, vol. 18, no. 2, pp. 310–321, 2009.